Double ionization of helium by ion impact analyzed using four-body Dalitz plots

M. F. Ciappina
Max Planck Institute for the Physics of Complex Systems, Nöthnizer Straße 38, D-01187 Dresden, Germany

M. Schulz
Physics Department and Laboratory for Atomic, Molecular and Optical Research, Missouri University of Science and Technology, Rolla, Missouri 65409, USA

T. Kirchner
Institut für Theoretische Physik, TU Clausthal, Leibnizstraße 10, D-38678 Clausthal-Zellerfeld, Germany

D. Fischer
Max-Planck-Institut für Kernphysik, Saupfercheckweg 1, D-69117 Heidelberg, Germany and Atomic Physics, Stockholm University, Alba Nova, S-106 91 Stockholm, Sweden

R. Moshammer and J. Ullrich
Max-Planck-Institut für Kernphysik, Saupfercheckweg 1, D-69117 Heidelberg, Germany
(Received 26 February 2008; published 13 June 2008)

We have performed experimental and theoretical studies of double ionization of helium by 6 MeV proton impact using a recently developed tool, four-particle Dalitz plots [Schulz *et al.*, J. Phys. B **22**, 3091 (2007)] which enable the representation of multiple differential cross sections as a function of all four fragments in a single spectrum without loss of any part of the total cross section. As a result, the relative importance of the various interactions between the fragments can be studied in great detail. Comparisons of experimental data with theoretical first-order calculations and simulations for the higher-order (TS-2) process show that elastic scattering between the heavy particles is surprisingly strong. For a large fraction of collision events, the final-state electron momenta are small compared to the momenta of the heavy particles. Our results suggest that an uncorrelated double ionization mechanism, involving two independent interactions of the projectile with both electrons, is significantly more important than previously expected for such fast collisions.

DOI: 10.1103/PhysRevA.77.062706 PACS number(s): 34.50.Fa, 34.10.+x

I. INTRODUCTION

The importance of studying atomic breakup processes for advancing our understanding of the fundamentally important few-body problem has been frequently pointed out; see, e.g., [1,2]. In the case of three-body fragmentation, e.g., single ionization (SI) of hydrogen or helium by charged-particle impact, the theoretical description has made impressive progress in recent years (e.g., [2–7]). In particular, measured fully differential cross sections (FDCS), which offer the most sensitive tests of theoretical models, can now basically be reproduced, except for some specific kinematic conditions [1], highly-charged-ion impact [8–10], and slow ion impact [11,12] (for a recent review see also [13]).

In four-body fragmentation processes involving a transition of two electrons, e.g., double ionization (DI) of helium by charged-particle impact, a particularly interesting aspect of the few-body problem is the role of correlation effects between the two electrons. Two DI mechanisms involving electron-electron correlations are usually discussed [14]: in one, dubbed two-step one-projectile-electron interaction two-step-one (TS-1) projectile-electron interaction, the projectile interacts with only one electron, which subsequently interacts with the second electron leading to the ejection of both electrons. In the second mechanism, called shake-off (SO), the projectile also interacts with only one electron directly. The resultant ejection of the electron may leave the residual He^+ ion in a state which is not an eigenstate of the Hamiltonian. Therefore, this state has a nonzero overlap with the continuum so that the second electron can be ejected with some finite probability. In terms of the projectile–target-atom interaction both TS-1 and SO are first-order processes. DI without any electron-electron correlations can occur only in second (and higher) order. In the second-order process, which is referred to as two-step two (TS-2) projectile-electron interaction, the projectile interacts with each electron independently.

The literature on measured data on DI is not nearly as comprehensive as for SI. In the case of electron impact FDCSs were obtained only by two groups [15,16] and for ion impact only one data set for nearly fully differential cross sections is available [17]. The qualitative features of these data are quite similar to photo-double-ionization and can to a large extent be described by a combination of a Coulomb repulsion between the two electrons in the continuum and the dipole selection rule prohibiting back to back emission of electrons with equal energy originating from the $1s^2$ ground state of helium. However, it is very difficult to extract information regarding the relative importance of the various DI mechanisms described above because it is not known with sufficient accuracy which mechanism leads to which characteristic features in the FDCS. Fischer *et al.* concluded indirectly that for electron impact TS-2 is somewhat more im-

portant than for proton impact at similar initial projectile velocity [17].

In spite of the tremendous power of analyzing FDCSs there are also some important drawbacks. First, experimental data for FDCS cover only a tiny fraction of the total cross section. As a result, features that appear to be very pronounced in the FDCSs for selected kinematic conditions may be insignificant in the total cross sections and vice versa. Consequently, it is difficult to evaluate the relative overall importance of the various DI mechanisms based on FDCSs. Second, using conventional plotting techniques, the FDCSs cannot be presented as a function of all collision fragments in a single spectrum. It is therefore practically impossible to analyze the correlation between all final-state particles simultaneously in the collision dynamics. These disadvantages of FDCSs were recently addressed by a new data analyzing technique which is based on four-particle Dalitz (4D) plots [18]. These plots are basically an extension of *conventional* Dalitz plots, originally introduced in particle physics to analyze three-body decays [19], to four-body fragmentation processes. The tremendous power of three-particle Dalitz plots has readily been demonstrated in atomic physics as well in studies of a broad variety of processes such as three-body fragmentation of molecules [20–22], single [23–25] and triple ionization [26] of atoms by charged-particle impact, or mutual ionization of both collision partners [27]. In a 4D plot, the data are presented in a tetrahedral coordinate system (compared to an equilateral triangle in regular Dalitz plots), where each tetrahedron plane represents one of the four fragments. The perpendicular distances of a given data point (which can occur only in the inner region of the tetrahedron) to the four planes represent the relative squared momenta of the four particles $\pi_i = p_i^2 / \Sigma p_j^2$, where in the case of the scattered projectile the momentum transfer to the target atom $\mathbf{q}$ is used instead of the total final-state projectile momentum.

In a 4D plot multiple differential cross sections are presented as a function of all collision fragments simultaneously in a single spectrum without loss of any part of the total cross section (given by the integral of the 4D plot). The disadvantages of FDCSs mentioned above are thus overcome. However, the obvious disadvantage is that the degree of differentiality is lower than in FDCSs, and 4D plots should therefore be viewed as a powerful complementary rather than competitive tool to FDCSs. Additional information can be obtained by generating the 4D plots for selected momentum components. Using this technique to analyze simultaneous electron ejection from both collision partners in $H^- + He$ collisions, it was recently demonstrated that some of the interactions involved in the collision dynamics leave their footprint only in specific coordinates [18].

In calculating 4D spectra, theory faces a serious problem which is usually not as severe for more *conventional* spectra. Total and differential cross sections of lower degree than FDCSs are normally obtained by integrating the latter over the appropriate kinematic parameters. Typically, measured spectra correspond to cross sections differential in parameters (e.g., ejected electron energy and angles, projectile scattering angle, etc.), which are part of a *natural* coordinate system used in theoretical models such that a degree of symmetry as high as possible is achieved. The integration of the FDCSs can then often be performed partly analytically or at least the required numerical efforts are minimized.

The four Dalitz coordinates are not *natural* in this sense and only a low degree of symmetry can be taken advantage of. Theoretical regular Dalitz plots (for three particles) were recently presented for SI of helium by ion impact [24]. However, the extra final-state particle in DI makes the analysis much more complex. Furthermore, the theoretical description even of the FDCSs is a much more challenging problem for DI than it is for SI. At present, it therefore seems hopeless to calculate 4D spectra by direct integration of the FDCS. One possible way out of this theoretical predicament is offered by the Monte Carlo event generator (MCEG) method which was recently introduced to atomic physics [28]. In this technique only the calculation of the FDCS is required, regardless of what type of cross section the investigator wishes to analyze. Based on these FDCSs a large number (typically around 1×10^6) of collision events leading to the process of interest (here DI) is simulated, or in other words the information provided by the detectors in an experiment is simulated. The kinematically complete information, i.e., the momentum components of the collision fragments, is then stored in an event file similar to the one obtained in the experiment. This event file can then be analyzed in precisely the same way as experimental data, i.e., whatever cross section can be extracted from the experiment is extractable from theory as well. In the case of SI this method was recently used to fully include the experimental resolution in theory [28] and to convolute the calculated cross sections with elastic scattering between the projectile and the residual target ion [29].

In this paper we present both measured and calculated 4D plots for DI in 6 MeV $p+He$ collisions. The theoretical plots were obtained using the MCEG technique described above. Although the prohibitively complex direct integration of the FDCS is avoided in this method, the generation of the event file is still very computer-time demanding. It is therefore currently not feasible for numerically intensive models and we applied it only to first-order type of calculations including electron-electron correlations. Furthermore, such spectra were generated by modeling DI in terms of two independent SI events. Extrapolating the rapidly increasing computer power to the future, performing such calculations with more sophisticated models should become possible not too long from now. Nevertheless, even the comparison of our measured data with the simulation of DI in terms of two independent SI events and with our relatively simple theoretical models readily provides surprisingly rich information about the DI collision dynamics. Perhaps the most significant result we report here is strong indications that TS-2 is much more important than previously assumed for this large projectile velocity.

II. EXPERIMENT

The experiment was performed at the 12 MV tandem Van de Graaff accelerator at the Max–Planck-Institut für Kernphysik in Heidelberg. A pulsed 6 MeV proton beam with a pulse length of about 1 ns and a repetition rate of 680 kHz

intersected with a cold (1.5 K) He beam from a supersonic gas jet. The recoil ions and the ionized electrons were extracted in the longitudinal direction (defined by the initial projectile direction) by a weak electric field of 2.3 V/cm. Their momentum vectors and the recoil charge state were determined by using position-sensitive detectors and time-of-flight techniques, where a fast signal from the projectile beam pulser served as a timing reference

A uniform magnetic field of 14 G confined the transverse motion of the electrons so that all electrons with a transverse momentum of less than 2 a.u. were guided onto the detector. For each DI event both electrons were detected simultaneously with a single detector employing a multihit technique (dead time≈10 ns). From the electron momenta it is straightforward to calculate the emission angles. In the data analysis losses due to the limited acceptance were carefully accounted for. The momentum components of the scattered projectiles are deduced in the data analysis from momentum conservation.

A thorough analysis of the resolution of all momentum components (electrons and recoil ions) in a kinematically complete experiment was recently performed for SI of helium by 100 MeV/amu C^{6+} impact [28,29]. It was found that the main contribution to the experimental overall uncertainties is due to the temperature of the target beam and the size of the interaction volume (i.e., the overlap of the projectile and target beam). In the present experiment the target temperature was about the same as in Ref. [29], but the size of the interaction volume was about a factor of 2 larger. However, in the momentum resolution of the recoil ions this larger size is partly compensated by the smaller extraction voltage used in this experiment. Furthermore, the momentum resolutions depend on the momenta themselves and therefore averaged values are provided. In the longitudinal (z) direction they are ± 0.075 and ± 0.005 a.u. for the recoil ion and for the electron, respectively. In the direction of the jet expansion (y direction), the corresponding numbers are ± 0.25 and ± 0.15 a.u., and for the x direction ± 0.1 and ± 0.05 a.u., respectively. Since the momentum resolution of the electrons is small compared to that of the recoil ion, the projectile momentum resolution is essentially the same as for the recoil ions.

III. DATA ANALYSIS

A thorough description of the 4D plots and their generation from Cartesian momentum components of the collision fragments was provided in [18] and will not be repeated here with the same level of detail. In short, as mentioned above, the data are presented in a tetrahedral coordinate system and can occur only in the inner region of the tetrahedron. Each tetrahedral plane represents one of the four final-state particles. The perpendicular distance of a specific data point to the four planes determines the relative squared momenta $\pi_i = p_i^2 / \Sigma p_j^2$ of the four collision fragments.

Since the momentum transfer is given by the sum of the momenta of the two ejected electrons $(\mathbf{k}_1, \mathbf{k}_2)$ and of the recoil ion $(\mathbf{p}_{\mathrm{rec}})$, the quantity $-\mathbf{q}+\mathbf{k}_1+\mathbf{k}_2+\mathbf{p}_{\mathrm{rec}}$ is zero. Considering that the Dalitz coordinates contain the momenta only in squared form, this condition has the same effect on the 4D plots as $\mathbf{q}+\mathbf{k}_1+\mathbf{k}_2+\mathbf{p}_{\mathrm{rec}}=\mathbf{0}$, i.e., if the 4D plots were generated using $-\mathbf{q}$ instead of $\mathbf{q}$ in the π_i's, the plot would not change. For the latter condition, in turn, it is easy to see that the entire inner region of the tetrahedron is not kinematically allowed: for example, for any corner of the tetrahedron, where three planes intersect, three of the four momenta are simultaneously zero, i.e., the condition that the summed momentum of all four momenta is zero cannot be satisfied.

A 4D plot can be generated using a standard Cartesian coordinate system by employing the following transformations [18]:

$$x = \pi_1, \quad y = \frac{1}{\sqrt{8}}(3\pi_2 + \pi_1), \quad z = \sqrt{\frac{3}{2}}(\pi_3 + 0.5\pi_2 + 0.5\pi_1). \tag{1}$$

It should be noted that these transformations also entail a phase space transformation of the cross sections such that, for a uniform distribution in Cartesian momentum space, the 4D plot will be strongly peaked in the center of the tetrahedron [18]. Therefore, structures near the center of the 4D plot could be merely due to this phase space transformation; however, any structures near the surface of the tetrahedron have a deeper significance.

IV. THEORETICAL FRAMEWORK

A. Fully differential cross sections in the first Born approximation

We treat DI within the first Born approximation (FBA). Since it contains the projectile-atom interaction only to first order, DI is only possible through a mechanism involving some form of electron-electron correlation (SO or TS-1), i.e., contributions from TS-2 are neglected in our calculations. Three models are employed which all use the same initial state incorporating part of the radial correlation and which differ only in the description of the final state.

The FDCS differential in the momentum of the two ejected electrons $\mathbf{k}_1$ and $\mathbf{k}_2$ and in the transverse component of the momentum transfer $\mathbf{q}$, i.e., $\mathbf{q}_\perp$, with $\mathbf{q}=\mathbf{q}_\perp+q_z\hat{\mathbf{v}}$ and $\mathbf{q}_\perp \cdot \hat{\mathbf{v}}=0$, $\hat{\mathbf{v}}$ being the direction of the projectile velocity $\mathbf{v}$, can be written as

$$\frac{d^8\sigma}{d\mathbf{k}_1 d\mathbf{k}_2 d\mathbf{q}_\perp} = \frac{(2\pi)^4}{v^2}|T_{if}|^2, \tag{2}$$

where we have reduced the dimensionality using the energy conservation δ function $\delta(E_i - E_f)$, E_i (E_f) being the total initial (final) energy of the system. In ion-atom collisions the relation $q_z = \Delta\epsilon / v$ is satisfied to a very good approximation. Here, the projectile energy loss is given by $\Delta\epsilon = k_1^2/2 + k_2^2/2 + |\varepsilon_i|$, where ε_i is the total binding energy of the helium atom.

Within the FBA, the transition amplitude T_{if} in the prior form is given by (see, e.g., [30])

$$T_{if} = \langle \Psi_f^{(-)} | \hat{V} | \Psi^0 \rangle \tag{3}$$

with the initial (final) state wave function Ψ_0 ($\Psi_f^{(-)}$) and the perturbation $\hat{V}$, which consists of the Coulomb interactions

between the incoming projectile and each of the constituents of the helium atom, i.e., both electrons and the nucleus.

We approximate the initial state Ψ_0 by a plane wave of momentum $\mathbf{K}_i$ for the incoming projectile $\Psi_{\mathbf{K}_i}$ and a two-electron wave function ϕ_0 that represents the helium ground state

$$|\Psi_0\rangle = |\Psi_{\mathbf{K}_i}\rangle|\phi_0\rangle. \tag{4}$$

Among the numerous models to represent the latter we choose the following ansatz which uses two different effective charges to model the screening of the atomic nucleus experienced by the *outer* electron and caused by the *inner* one:

$$\phi_0(\mathbf{r}_1,\mathbf{r}_2) = N(e^{-Z_a r_1}e^{-Z_b r_2} + e^{-Z_b r_1}e^{-Z_a r_2}). \tag{5}$$

The charges Z_a and Z_b are calculated variationally and have the values 2.183 171 and 1.188 530, respectively. This model yields the ground-state energy $\varepsilon_i = -2.8757$ a.u. [31], which is below the Hartree-Fock result $\varepsilon_i = -2.8617$ a.u. for the $1s^2$ configuration. In this sense (radial) correlations are included to some extent in the initial state [30].

The final-state wave function is assumed to be of the form

$$|\Psi_f^-\rangle = |\Psi_{\mathbf{K}_f}\rangle|\phi^{(-)}_{\mathbf{k}_1,\mathbf{k}_2}\rangle, \tag{6}$$

where $\Psi_{\mathbf{K}_f}$ represents a plane wave for the outgoing projectile with momentum $\mathbf{K}_f$ and $\phi^{(-)}_{\mathbf{k}_1,\mathbf{k}_2}$ is a two-electron continuum eigenfunction of the helium atom Hamiltonian. Within the FBA the integral over the projectile coordinate can be calculated directly, and consequently we can write the transition amplitude T_{if} as

$$T_{if} = \frac{Z_P}{2\pi^2 q^2}(Z_T M_0 - M_1 - M_2) \tag{7}$$

with momentum transfer $\mathbf{q} = \mathbf{K}_i - \mathbf{K}_f$, projectile charge Z_P, target nuclear charge $Z_T = 2$, and

$$M_0 = \int d\mathbf{r}_1 \int d\mathbf{r}_2 \phi^{(-)*}_{\mathbf{k}_1,\mathbf{k}_2}(\mathbf{r}_1,\mathbf{r}_2)\phi_0(\mathbf{r}_1,\mathbf{r}_2), \tag{8}$$

$$M_1 = \int d\mathbf{r}_1 \int d\mathbf{r}_2 \phi^{(-)*}_{\mathbf{k}_1,\mathbf{k}_2}(\mathbf{r}_1,\mathbf{r}_2)e^{i\mathbf{q}\cdot\mathbf{r}_1}\phi_0(\mathbf{r}_1,\mathbf{r}_2), \tag{9}$$

$$M_2 = \int d\mathbf{r}_1 \int d\mathbf{r}_2 \phi^{(-)*}_{\mathbf{k}_1,\mathbf{k}_2}(\mathbf{r}_1,\mathbf{r}_2)e^{i\mathbf{q}\cdot\mathbf{r}_2}\phi_0(\mathbf{r}_1,\mathbf{r}_2). \tag{10}$$

In a strict sense the contribution of M_0 to the T matrix should vanish in the FBA because of the orthogonality of the initial and final electronic states. However, it should be noted that with the way we model these states they are not exactly orthogonal. As a result, the T matrix contains some contributions from elastic scattering between the projectile and the target nucleus. However, a test calculation confirmed that these contributions are insignificant because the nonorthogonality is small.

To proceed further it is necessary to specify the two-electron wave function $\phi^{(-)}_{\mathbf{k}_1,\mathbf{k}_2}(\mathbf{r}_1,\mathbf{r}_2)$. There exist several models to deal with the two-electron continuum (see, e.g., [32]) in approximate fashion. We choose three of them to study the DI process. The first model, which serves also as a reference, is a symmetrized product of two one-electron scattering eigenstates with incoming boundary conditions $\phi^{(-)}_{\mathbf{k}}(\mathbf{r})$ of the bare helium nucleus. This electronic wave function reads

$$\phi^{(-),2C}_{\mathbf{k}_1,\mathbf{k}_2}(\mathbf{r}_1,\mathbf{r}_2) = \frac{1}{\sqrt{2}}[\phi^{(-)}_{\mathbf{k}_1}(\mathbf{r}_1)\phi^{(-)}_{\mathbf{k}_2}(\mathbf{r}_2) + \phi^{(-)}_{\mathbf{k}_2}(\mathbf{r}_1)\phi^{(-)}_{\mathbf{k}_1}(\mathbf{r}_2)] \tag{11}$$

and is known as the 2–Coulomb (2C) model. It describes the two one-electron-nucleus subsystems exactly, but neglects the interaction between the electrons completely, i.e., this model contains electron-electron correlations only in the initial state. The 2C model was used extensively in the past in studies of electron impact ionization of helium [33]. Due to the absence of electron-electron correlations in the final state, it leads to an unphysical preference for both electrons to be emitted into the same direction, a feature that was pointed out by several authors (see, e.g., [34] and references therein).

In the second model we incorporate the asymptotic boundary conditions of the three-body Coulomb problem, i.e., of the two ionized electrons and the residual target ion. This can be accomplished by adding a third Coulomb distortion to model the electron-electron interaction and thus improve the representation of the dynamics of the system at large interparticle distances. A variety of model wave functions have been proposed in the field of electron impact ionization, e.g., the 3C or Brauner-Briggs-Klar wave function [35]. These models represent the three-body asymptotic state in terms of combinations of two-body subsystems, which are in turn described by suitable effective one-body wave functions. The evaluation of the ionization T matrix elements with this three-body wave function is cumbersome, since it requires a substantial numerical effort, thereby making subsequent numerical calculations of differential cross sections impractical [35]. In order to avoid these difficulties a simplified version of the 3C ansatz was suggested, in which the relative Coulomb scattering wave function of the two-electron subsystem is replaced by its value at zero spatial distance. The explicit expression for this wave function can be written as [36]

$$\phi^{(-),2C+}_{\mathbf{k}_1,\mathbf{k}_2}(\mathbf{r}_1,\mathbf{r}_2) = \frac{1}{\sqrt{2}}[\phi^{(-)}_{\mathbf{k}_1}(\mathbf{r}_1)\phi^{(-)}_{\mathbf{k}_2}(\mathbf{r}_2) + \phi^{(-)}_{\mathbf{k}_2}(\mathbf{r}_1)\phi^{(-)}_{\mathbf{k}_1}(\mathbf{r}_2)] \times \alpha(k_{12}), \tag{12}$$

where

$$\alpha(k_{12}) = e^{-\pi\xi_{12}}\Gamma(1 - i\xi_{12}), \quad \xi_{12} = \frac{Z_{12}}{k_{12}}, \tag{13}$$

with $k_{12} = |\mathbf{k}_1 - \mathbf{k}_2|$ being the relative momentum between the two electrons and $Z_{12} = 1$ represents the case of *static screening* (see the discussion below). In the transition probabilities and cross sections, the quantity

$$|\alpha(k_{12})|^2 = \frac{2\pi\xi_{12}}{e^{2\pi\xi_{12}} - 1} \tag{14}$$

appears as a prefactor. Equation (14), known as the Gamov factor, was used extensively in investigations of DI by electron and ion impact. It suppresses exponentially the probability to find both ionized electrons with close momenta, but ensures that electrons with very different momenta move independently.

The choice $Z_{12}=1$ yields too strong a repulsion between electrons with low emission energies, and consequently the cross sections near threshold are underestimated. In our third model we address this drawback by introducing effective charges that depend on the electron momenta [37–40]. Different explicit forms for this dependence have been proposed and applied to different processes, especially in electron-induced ionization processes. These models are known generically as *dynamic screening* approaches. Very recently, a simplified derivation of dynamic screening was proposed and used to describe $(e,3e)$ reactions [41], and furthermore applied to model the correlation function in DI by ion impact [42]. Following Ref. [41], we use the effective charge

$$Z_{12} = 1 - \frac{k_{12}^2}{(k_1 + k_2)^2} \tag{15}$$

in Eq. (14). We label our models as follows: model I refers to Eq. (11), model II to the one which uses the static charge $Z_{12}=1$, and model III to the one which uses the screened charge (15) in Eq. (14). In all cases discussed below the initial-state wave function (5) has been used.

B. The Monte Carlo event generator method

As mentioned above, the second important step, apart from calculating the FDCS for DI, is to use the MCEG technique to generate an event file with which the 4D plots can be generated using an identical analysis as for the experimental data. A detailed explanation of the MCEG procedure can be found in [28], where the method was used to deal with SI by ion impact. Consequently, we give only a brief description of the numerical procedure to calculate the event files for DI, and we emphasize the differences from the SI case.

In DI by ion impact, the event file contains seven independent momentum components which are required to fully determine the kinematics, i.e., three components for each of the ejected electrons $(k_1^x,k_1^y,k_1^z,k_2^x,k_2^y,k_2^z)$ and one component of the momentum transfer (q_x). We use a coordinate system in which x is pointing along the transverse component of $\mathbf{q}$ so that $q_y=0$ for all events. The component of $\mathbf{q}$ along the z axis, defined by the initial beam direction, is readily determined by the sum energy of both ejected electrons (see previous section) and is thus not needed.

For all momentum components of both electrons the collision kinematics is restricted to a range from −2 to 2 a.u. Furthermore, for the transverse component of the momentum transfer q_x the range is between 0 and 2 a.u. The Monte Carlo generated events are selected using a simple rejection method, where the following cycle is repeatedly executed until a sufficiently large sample of good events has been generated. (i) A set of eight random numbers is chosen, seven of which represent a point in the seven-dimensional momentum phase space $(k_1^x,k_1^y,k_1^z,k_2^x,k_2^y,k_2^z,q_x)$ and are uniformly distributed within the limits stated above. The eighth random number u is uniformly distributed in the interval (0,1). (ii) The cross section is calculated at the randomly selected point $(k_1^x,k_1^y,k_1^z,k_2^x,k_2^y,k_2^z,q_x)$ from the theoretical model, in our case FBA-type models with and without the inclusion of electronic correlation in the final state. (iii) The random number u is compared with the normalized cross section $\tilde{\sigma}(k_1^x,k_1^y,k_1^z,k_2^x,k_2^y,k_2^z,q_x) = \sigma(k_1^x,k_1^y,k_1^z,k_2^x,k_2^y,k_2^z,q_x)/\sigma_{\max}$ where $\sigma_{\max}$ is the maximum of the cross section within the selected seven-dimensional phase space. In this way $\tilde{\sigma}$ ranges between zero and one. (iv) If $u<\tilde{\sigma}$ we consider the event represented by the seven momenta a good event and store it in the event file. On the other hand, the event is discarded if $u>\tilde{\sigma}$.

As the cross section drops more rapidly toward larger electron momenta and momentum transfers, as in the case of SI, this method becomes quite inefficient, i.e., many events are rejected so that a lot of random numbers need to be generated until a sufficiently large event file is obtained. The efficiency of the rejection method could be improved significantly by modifying the weight of the randomly selected number u from a uniform to another distribution, which is a better match to the cross section. However, this last task is difficult to achieve in our seven-dimensional phase space and consequently we have used the usual random number generators with uniform distributions.

It should be noted that it is necessary to assure the *quality* of the pseudorandom number generator in our numerical scheme. One measure of the randomness is the period of the random sequence, and to this end we have adopted a portable random number routine with a period around 2×10^{18} that is enough for our purposes [43]. Typically, the event files contain about 1×10^6 valid DI events. To obtain this quantity of events is certainly a computational challenge, since the *acceptance* for DI events is even smaller than for the case of SI. Out of 2×10^{10} trials only approximately 600 events survived the rejection and were stored in the file. Consequently, to obtain the full quantity of events it is necessary to run the single routine several hundreds of times. Using parallel programming techniques implemented in a distributed computational system, we were able to handle this problem in a reasonable time (approximately five days for each model).

V. EXPERIMENTAL RESULTS

An experimental 4D plot is shown in Fig. 1(a) for DI of helium by 6 MeV proton impact. This and all following plots are shown with an offset of 7% of the maximum number of counts in the spectrum. Without this offset the spectra would be overloaded with data points so that the prominent structures would be very difficult to identify. The ejected electrons are represented by the front and bottom planes, the recoil ion by the back plane and the scattered projectile (i.e., the momentum transfer) by the right plane. At the intersection lines of two tetrahedral planes, the momenta of the par-

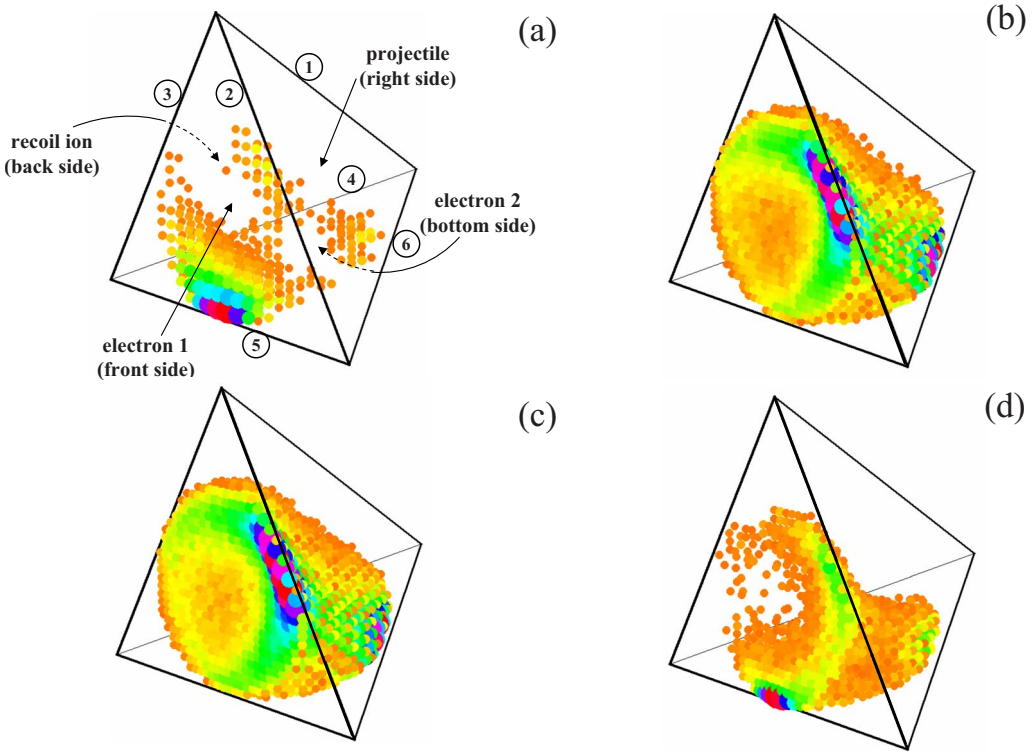

FIG. 1. (Color online) Experimental and theoretical 4D plots for DI of helium by impact of 6 MeV protons. (a) Experimental 4D plot, (b) 4D plot using the TS-2 simulation without any convolution, (c) 4D plot using the TS-2 simulation convoluted only with resolution, and (d) 4D plot using the TS-2 simulation convoluted with both experimental resolution and elastic scattering. For all the 4D plots the three components of the particle momenta were used (see text).

ticles represented by these planes are zero and the momentum exchange in the collision occurs only between the other two particles. We therefore associate events falling on these intersection lines with binary interactions and they are labeled 1 through 6 in Fig. 1(a) for easier reference in the text.

The dominant feature in the experimental 4D plot of Fig. 1(a), similar to what was observed in Ref. [18], is a peak at the intersection line between the planes representing the two ejected electrons (line 5). For this region, the momenta of the electrons are small compared to the recoil-ion momentum and to $\mathbf{q}$, i.e., the momentum exchange occurs predominantly between the two heavy particles. Therefore, just as in simultaneous electron ejection from both collision partners in relatively slow 200 keV H^-+He collisions, elastic scattering between the projectile and the target nucleus surprisingly plays a major role for the momentum balance in doubly ionizing collisions even at the very small perturbation parameter $\eta \approx 0.065$ (projectile charge to velocity ratio) realized for the present collision system. Non-negligible peak structures are also observed near intersection lines 2 and 6 representing binary interactions between the target nucleus and one of the ejected electrons. As pointed out in Ref. [18], these structures partly represent a residue of the momentum distribution of the target atom in the initial ground state and we therefore refer to them as *internal correlations*. However, as we will show in the next section, the repulsion between the electrons in the continuum may also contribute in this region. Finally, weak contributions are found near intersection lines 3 and 4 representing binary interactions between the projectile and one electron.

It is interesting to note that binary electron-electron interactions, represented by intersection line 1, are almost completely absent in the 4D plots. However, this does not imply by any means that electron-electron correlation effects are unimportant. In sharp contrast to simultaneous electron ejection from both collision partners studied in Ref. [18] DI cannot proceed through an electron-electron interaction alone, but rather an interaction of the projectile with at least one electron is required. On the other hand, the minimum momentum transferred by the projectile in DI is given by $q_{\min} = \varepsilon_i / v = 0.19$ a.u. [44], where ε_i is the total binding energy of 79 eV. Binary electron-electron interactions with negligible momentum transfer and negligible recoil-ion momentum are therefore unlikely. In the next section we will discuss in which regions of a 4D plot signatures of electron-electron correlations might be expected.

As a first attempt to interpret the features observed in the 4D plot we analyze DI in terms of a simulation of the TS-2 mechanism convoluting two independent SI events. We realize that for the fast collisions investigated here TS-2 is not necessarily expected to be the most important mechanism. However, such an analysis is nevertheless useful because it provides valuable information about the signatures of TS-2 to be expected in the 4D plots. The signatures of first-order correlated DI processes (SO and TS-1) we will explore in the next section using our theoretical models.

The convolution of two independent SI events can be performed in various ways. One possibility is to convolute SI of neutral helium (with an ionization potential of 24.6 eV) with SI of He^+ (with an ionization potential of 54.4 eV), which we

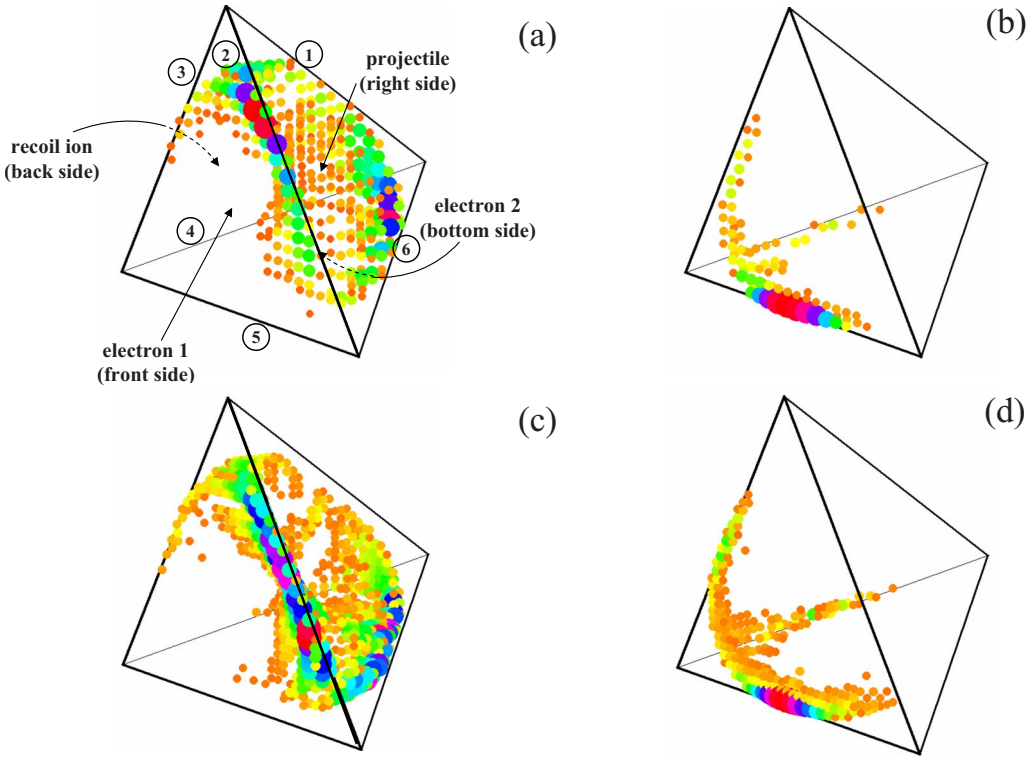

FIG. 2. (Color online) (a) Experimental 4D plot for only the longitudinal components of the particle momenta, (b) as in (a) but for the transverse component in the scattering plane, (c) 4D plot using the TS-2 simulation for only the longitudinal components of particle momenta, and (d) as in (c) but for the transverse component in the scattering plane. For cases (c) and (d) the TS-2 event files were convoluted with both experimental resolution and elastic scattering.

call the independent event model [45]. Another possibility is to treat the two electrons as completely equivalent, i.e., assuming that they equally share the total two-electron binding energy of the helium ground state, and to consequently convolute two SI events assuming an ionization potential of 39.5 eV for each electron [46]. We refer to this approach as the independent electron model. Reasonable arguments can be made for both approaches and it is not immediately clear which one is more appropriate. We therefore employed both methods.

Since we only have experimental data for SI of neutral helium, we performed the convolution using calculated SI cross sections for ionization potentials of 24.6, 39.5, and 54.4 eV, respectively, employing the FBA. The 4D plots were then calculated basically the same way as for our theoretical DI models. One important difference is that two calculations of the FDCS (one for each SI event) had to be done simultaneously. Another difference is that the x and z components of two momentum transfers (again, one for each SI event) were stored in the event file. Since the x direction was chosen to be the transverse component in the scattering plane (defined by the initial and final projectile momenta), the direction of the electron momentum and the momentum transfer in the xy plane had to be randomized for one of the two SI events. This accounts for the independent nature of the two SI events, which implies that all mutual angles between the electron emission planes for both events should occur with equal probability and that the scattering planes for the two SI events are generally not identical. The total momentum transfer for the simulated DI event is then simply the sum of the momentum transfers for the SI events. Final-state correlations were accounted for by rejecting simulated DI events with a probability given by the Gamov factor depending on the relative momenta between the two electrons. At this point, the 4D plots can be calculated exactly the same way as in the experimental data analysis and in the theoretical models. Although this simulation is not a rigorous representation of TS-2, for simplicity we nevertheless use this notation when we refer to it for the remainder of this paper.

The results of the TS-2 simulation are shown in Fig. 1(b). In this spectrum, and in all other spectra generated by the TS-2 simulation, we did not observe noticeable differences depending on whether the independent electron or the independent event model was used (in all cases the results of the independent event model are plotted). Before we compare to the experimental data, we study the influence of the experimental resolution on the 4D plots. To this end the TS-2 simulation was additionally convoluted with all known contributions to the experimental resolution following the method of Dürr *et al.* [28], and the result is shown in Fig. 1(c). Surprisingly, the resolution has no noticeable effect on the TS-2 simulation and the same behavior was also found when our theoretical models were convoluted with the resolution.[1] Figure 1(d) shows our TS-2 simulation convoluted with both the

[1]In contrast, a significant effect of the resolution on the angular distribution of the electrons was found, which will be described in a forthcoming presentation.

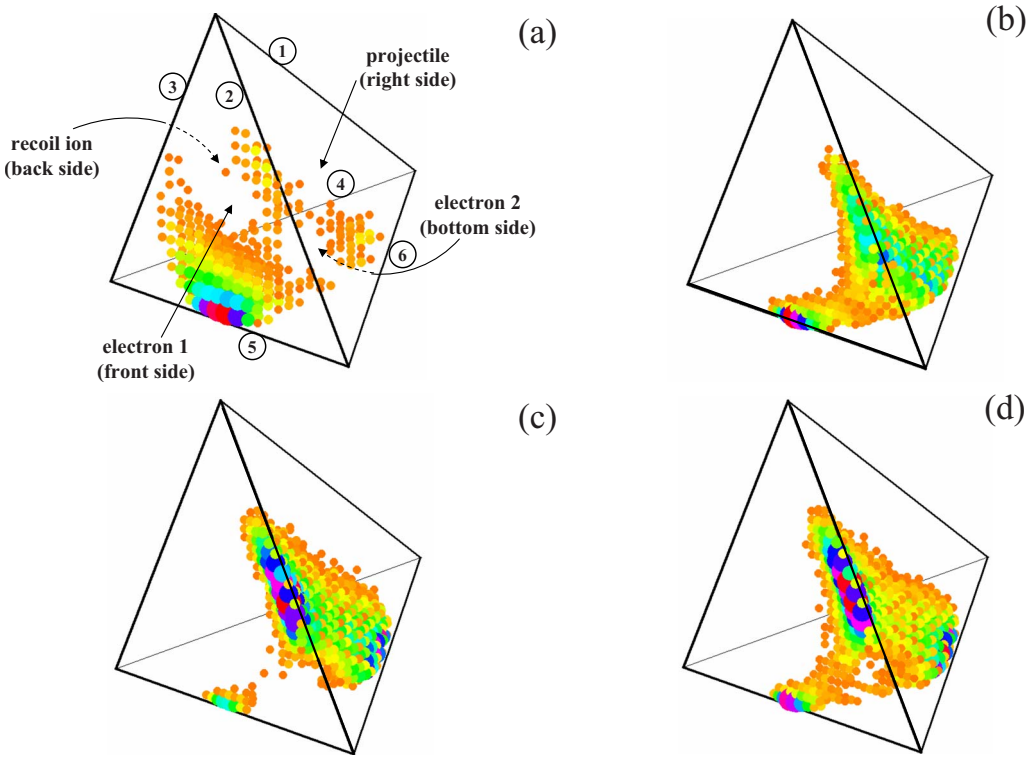

FIG. 3. (Color online) (a) Experimental 4D plot, (b) theoretical 4D plot for the model I (uncorrelated final-state model), (c) as in (b) for the model II (static screening model), and (d) as in (b) for the model III (dynamic screening model). For all the 4D plots the three components of the particle momenta were used and the theoretical models (b), (c), and (d) were convoluted with both experimental resolution and elastic scattering (see text).

experimental resolution and with elastic scattering (in the following referred to as *full convolution*) using the method of Schulz *et al.* [29]. Not surprisingly, the convolution with elastic scattering leads to a pronounced peak at intersection line 5 which, in fact, becomes the dominant feature in the 4D plot.

The spectrum with the full convolution is in surprisingly good qualitative agreement with the experimental data. More specifically, it reproduces that elastic scattering is the dominant feature, that the internal correlations lead to peak structures near intersection lines 2 and 6, and that some weak contributions from binary projectile-electron interactions are present (intersection lines 3 and 4). However, quantitatively there are some significant discrepancies. In particular, the internal correlations are overestimated by our simulation relative to elastic scattering.

Additional information about the DI collision dynamics can be obtained by generating 4D plots for specific momentum components of the final-state particles. In Fig. 2(a) such a spectrum is shown for the longitudinal components (i.e., the initial projectile beam direction) and in Fig. 2(b) for the transverse components in the scattering plane. For comparison, the corresponding spectra obtained from the TS-2 simulation are shown in Fig. 2(c) and 2(d), respectively. Note that the peak at intersection line 5 is strongly suppressed in the longitudinal plot (both in the experiment and in the simulation) because in elastic scattering the momentum exchange occurs almost exclusively in the transverse direction. For both components, especially the transverse component in the scattering plane, the qualitative agreement with the data is even better than for the three-dimensional momentum vectors.

The pronounced peak structure occurring at intersection line 5 (except for the longitudinal components) is readily associated with elastic scattering and is thus not a signature of a specific DI mechanism. In the longitudinal direction the internal correlations (intersection lines 2 and 6) in the simulation are much more pronounced than for the three-dimensional momenta, in accordance with the experimental data. Likewise, in the transverse direction in the scattering plane the binary projectile-electron interactions become much more important and now actually lead to a peak structure near intersection lines 3 and 4, again in accordance with the data. However, before we can conclude that these features are signatures of the TS-2 mechanism it is necessary to explore whether the 4D plots are even sensitive to the details of the DI collision dynamics. More specifically, in the next section we will analyze which features in the 4D plots emerge from first-order DI mechanisms like SO and TS-1 by comparing the experimental data to our theoretical models.

VI. COMPARISON TO THEORY AND DISCUSSION

In Fig. 3 we compare the 4D plots calculated with our various models with each other and to the experimental data for the total three-dimensional momentum vectors. In Fig. 3(a) we show the experimental data and Figs. 3(b), 3(c), and 3(d) represent the corresponding 4D plots for the theoretical

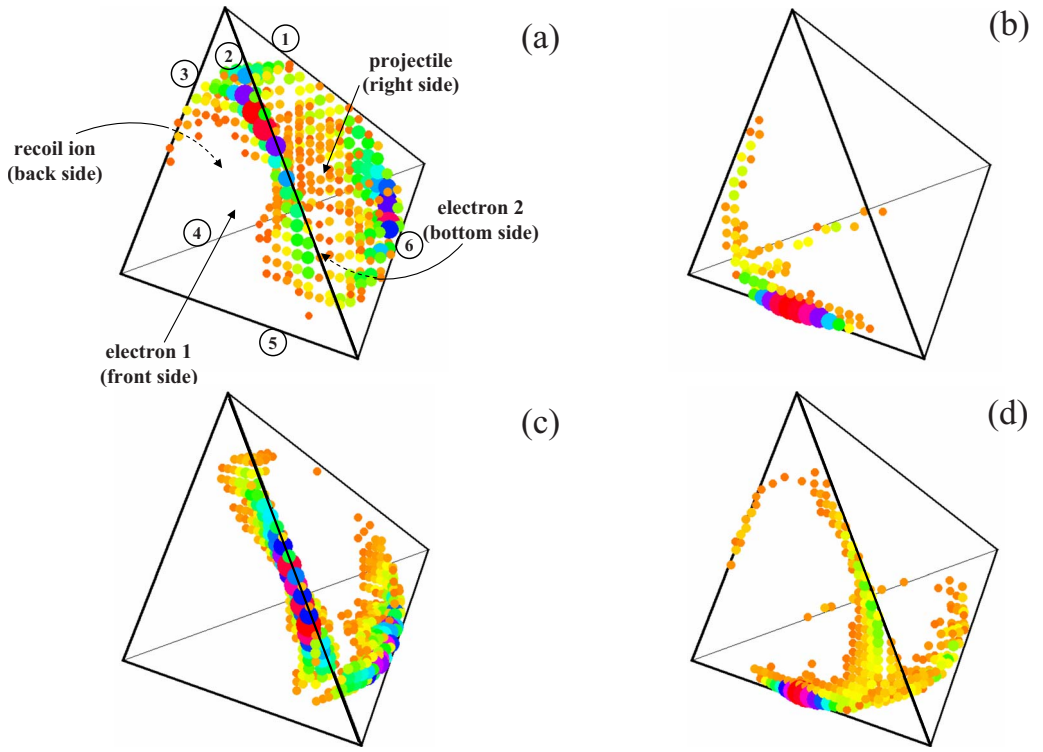

FIG. 4. (Color online) (a) Experimental 4D plot only for the longitudinal components of the particle momenta, (b) as in (a) but for the transverse component in the scattering plane, (c) theoretical 4D plot using the model III (dynamic screening model) only for the longitudinal components of the particle momenta, and (d) as in (c) but for the transverse component in the scattering plane. For cases (c) and (d) the theoretical event files were convoluted with both experimental resolution and elastic scattering.

models I, II, and III, respectively. Note that the theoretical models were fully convoluted with both experimental resolution and elastic scattering. For all three models most of the intensity occurs (apart from the elastic scattering peak at intersection line 5) along a plane parallel and very close to the plane representing the projectile. Here, the momentum transfer is small and in this region the internal correlation between the target nucleus and one or both electrons probably contributes significantly. We have checked that this feature also remains virtually unchanged if we turn off the initial-state correlation by choosing $Z_a=Z_b=27/16$ in Eq. (5). Given this insensitivity to the initial and final states and the absence of the feature in the TS-2 simulation, we attribute it to the representation of the reaction dynamics in terms of a first-order model, in which DI can only occur via electron-electron interaction. Note that this remains true even if completely uncorrelated states are used: in this case the electron-electron correlation is mimicked solely by the nonorthogonality of initial and final states in the transition amplitude. The data are much better described by the TS-2 simulation in that the intensity close to the projectile plane is generally much weaker than in theory and is significant only near the intersection lines with the two electron planes. This comparison suggests that the correlation in the reaction dynamics is significantly overemphasized by our theoretical first-order models.

Comparing the model without to those with final-state correlation, it appears that one effect of the electron-electron repulsion in the continuum is to favor a more asymmetric energy sharing among the electrons with one fast and one slow electron. This leads to the pronounced peak structures along intersection lines 2 and 6 which are much less pronounced in the model without final-state correlation. A similar effect is also seen in the TS-2 simulation: if the Gamov factor is *turned off* the structures along those lines become weaker (not shown). However, these maxima do not disappear completely because the internal correlation is still present. In the data the corresponding peak structures are even weaker than in the TS-2 simulation without Gamov factor. One reason could be that the final-state correlation is overestimated by the Gamov factor, even if it is used with a dynamic screening. In either case in a 4D plot signatures of the final-state correlation cannot be easily identified because they cannot be separated from the internal target correlation. As a summary of Fig. 3 we ascertain that all three theoretical models do not reproduce the experimental data as well as the TS-2 simulation.

In Fig. 4 the theoretical model accounting for the final-state correlation using dynamic screening (bottom panels) is compared to the experimental data (top panels) for the longitudinal direction [Figs. 4(a) and 4(c)] and for the transverse component in the scattering plane [Figs. 4(b) and 4(d)]. In the following, we will not discuss the other theoretical models because no major differences between the various calculations were found. For the longitudinal components much better qualitative agreement is achieved than for the three-dimensional momentum vectors. However, the data are still not as well reproduced as by the TS-2 simulation. For the

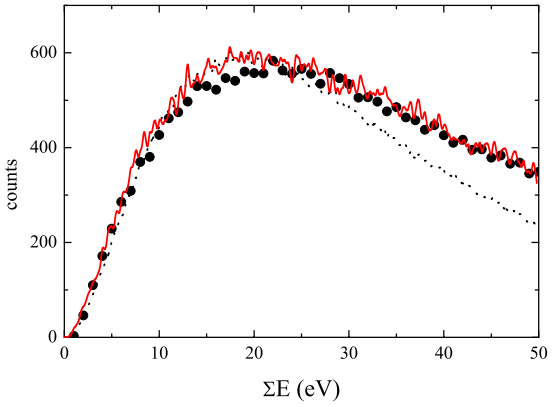

FIG. 5. (Color online) Spectra as function of the summed energy of both ionized electrons. Closed symbols, experimental data; solid line, TS-2 model convoluted with both elastic scattering and experimental resolution; dotted line, dynamic screening model convoluted with both elastic scattering and experimental resolution.

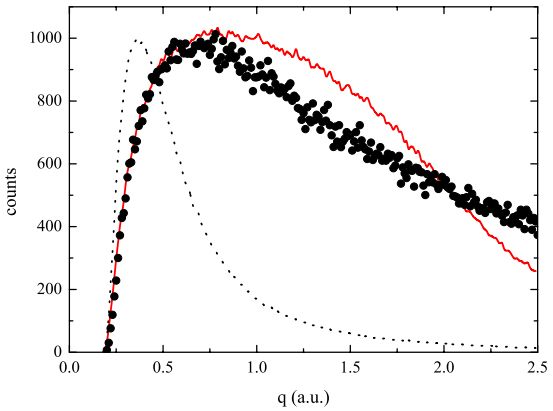

FIG. 6. (Color online) Spectra as function of the transverse momentum transfer component. Closed symbols, experimental data; solid line, TS-2 model convoluted with both elastic scattering and experimental resolution; dotted line, dynamic screening model convoluted with both elastic scattering and experimental resolution.

transverse components in the scattering plane, in contrast, major qualitative discrepancies are rather obvious. While both in the data and in the TS-2 simulation essentially no intensity is observed near the tetrahedral plane representing the projectile, in the calculation such contributions are quite significant. Therefore, for the scattering plane the overestimation of the correlation in the reaction dynamics appears to be particularly severe. A significant difference to the 4D plots for the three-dimensional momenta is that in the scattering plane (both for the transverse and for the longitudinal components) these contributions are restricted to regions near the intersection lines with the two planes representing the electrons. This suggests that either the internal target correlation or the final-state correlation (or both) are overestimated as well. Finally, we note one element of qualitative agreement with the data: as in the TS-2 simulation the contributions from binary interactions between the projectile and one electron (intersection lines 3 and 4) are reproduced at about the right intensity in the plot for the transverse components in the scattering plane.

The comparison of the data with the TS-2 simulation and with the theoretical models describing first-order DI mechanisms seems to strongly favor the TS-2 model. However, for two reasons it would be premature to conclude that DI is dominated by TS-2. First, our simulation does not represent a rigorous theoretical treatment of TS-2. For example, SI probabilities are convoluted to obtain the FDCS for DI when amplitudes should be considered. Furthermore, the propagation of the projectile in between interactions (in the Born series described by a Green's function) is not properly accounted for. Second, the much better agreement of the data with the TS-2 simulation compared to the theoretical models may just be a fortuitous anomaly of the 4D plots. It is therefore important to test the TS-2 simulations and the theoretical models by also comparing to other experimental spectra.

In Fig. 5 we present a measured spectrum of the sum energy of both ejected electrons in comparison to the TS-2 simulation (solid line) and the theoretical model using dynamic screening (dotted curve). The calculation is in reasonable agreement with the data; however, once again, the simulation fares even better and is in near perfect agreement with the data. A momentum transfer spectrum is shown in Fig. 6. Here, severe discrepancies between the calculation (dotted line) and the data are quite obvious. More specifically, the average momentum transfer predicted by theory is far too small. This seems to be the key problem in our theoretical model which can also, at least partly, explain the discrepancies in the 4D plots. The overestimation of the intensity along the intersection lines representing momentum exchange only between the target nucleus and one electron is consistent with the discrepancies in the momentum transfer spectrum. Furthermore, such discrepancies are to be expected if TS-2 plays an important role. Indeed, the TS-2 simulation is undoubtedly in much better agreement with the data than the calculation. Several other experimental spectra, like, e.g., angular distributions of the ejected electrons, were tested and in all cases the simulation is in better accord with the data than the calculation. With all the success of the TS-2 simulation it is important to keep its shortcomings in mind (see above). We therefore refrain from definite conclusions regarding the relative importance of the various DI mechanisms. On the other hand, the observation that the TS-2 simulation yields better, and generally good, agreement with the data in every tested spectrum is unlikely to be purely fortuitous and should thus not be ignored. A rigorous theoretical investigation of higher-order contributions to the DI cross sections is called for. 4D plots offer a powerful tool to study the contributions from the various DI mechanisms. Given the continuously increasing computational power calculations of 4D plots even with numerically more involved models should become feasible in the not too distant future.

VII. CONCLUSIONS

We have presented an experimental and theoretical study of double ionization of helium by fast proton impact. Our analysis is based on four-particle Dalitz plots, which were recently developed to investigate four-body fragmentation processes [18]. The unique feature of these spectra is that

they enable the plotting of multiple differential data as a function of all four final-state particles simultaneously in a single graph without loss of any part of the total cross section. As a result, 4D plots provide a comprehensive and yet detailed picture about the four-body fragmentation dynamics.

By comparing experimental data to a simulation of a higher-order DI process and to theoretical calculations on first-order DI processes we were able to identify some signatures of the various interactions contributing to the DI dynamics and of different DI mechanisms. For example, elastic scattering between the heavy particles leads to a surprisingly strong peak in the 4D plots in the region for which the electron momenta are small compared to the momenta of the heavy particles. The correlation in the dynamics which is inherent in the first-order DI models leads to large intensities close to the tetrahedral plane representing the projectile, i.e., it favors small momentum transfers, which is not observed in the experimental data. Our results suggest that our theoretical models significantly overestimate both correlation in the reaction dynamics and in the final state.

Perhaps the most significant observation in this work is that the TS-2 simulation generally yields nice qualitative agreement with the data and, in fact, reproduces the data much better than all of our theoretical first-order models. This is quite surprising because it was generally held that for such fast collisions first-order DI processes should be dominant. We pointed out the shortcomings of the TS-2 simulation from a rigorous theoretical point of view. Conclusions should therefore be drawn very cautiously. Nevertheless, we believe that the results presented imply sufficient significance to warrant a thorough scrutiny on the relative importance of the various DI mechanisms. To this end we are now developing sophisticated higher-order DI codes which treat first-and higher-order processes coherently. New calculations of 4D plots will then be performed as soon as the required computational resources become available.

ACKNOWLEDGMENTS

This work was supported by the National Science Foundation under Grant No. PHY-0652519 and by the Deutsche Forschungsgemeinschaft.

[1] M. Schulz, R. Moshammer, D. Fischer, H. Kollmus, D. Madison, S. Jones, and J. Ullrich, Nature (London) **422**, 48 (2003).
[2] T. N. Rescigno, M. Baertschy, W. A. Isaacs, and C. W. McCurdy, Science **286**, 2474 (1999).
[3] J. Röder, M. Baertschy, and I. Bray, Phys. Rev. A **67**, 010702(R) (2003).
[4] S. Jones and D. H. Madison, Phys. Rev. Lett. **81**, 2886 (1998).
[5] M. S. Pindzola and F. Robicheaux, Phys. Rev. A **54**, 2142 (1996).
[6] K. Bartschat, M. P. Scott, P. G. Burke, T. Stitt, N. S. Scott, A. N. Grum-Grzhimailo, S. Riordan, G. Ver Steeg, and T. I. Strakhova, Phys. Rev. A **65**, 062715 (2002).
[7] D. Madison, M. Schulz, S. Jones, M. Foster, R. Moshammer, and J. Ullrich, J. Phys. B **35**, 3297 (2002).
[8] M. Schulz, R. M. A. N. Perumal, and J. Ullrich, J. Phys. B **35**, L161 (2002).
[9] M. Foster, D. H. Madison, J. L. Peacher, and J. Ullrich, J. Phys. B **37**, 3797 (2004).
[10] R. T. Pedlow, S. F. C. O'Rourke, and D. S. F. Crothers, Phys. Rev. A **72**, 062719 (2005).
[11] M. Schulz, A. Hasan, N. V. Maydanyuk, M. Foster, B. Tooke, and D. H. Madison, Phys. Rev. A **73**, 062704 (2006).
[12] M. F. Ciappina, W. R. Cravero, and M. Schulz, J. Phys. B **40**, 2577 (2007).
[13] M. Schulz and D. H. Madison, Int. J. Mod. Phys. A **21**, 3649 (2006).
[14] J. H. McGuire, *Electron Correlation Dynamics in Atomic Collisions* (Cambridge University Press, Cambridge, England, 1997).
[15] I. Taouil, A. Lahmam-Bennani, A. Duguet, and L. Avaldi, Phys. Rev. Lett. **81**, 4600 (1998).
[16] A. Dorn, A. Kheifets, C. D. Schröter, B. Najjari, C. Höhr, R. Moshammer, and J. Ullrich, Phys. Rev. Lett. **86**, 3755 (2001).
[17] D. Fischer *et al.*, Phys. Rev. Lett. **90**, 243201 (2003).
[18] M. Schulz, D. Fischer, T. Ferger, R. Moshammer, and J. Ullrich, J. Phys. B **40**, 3091 (2007).
[19] R. H. Dalitz, Philos. Mag. **44**, 1068 (1953).
[20] L. M. Wiese, O. Yenen, B. Thaden, and D. H. Jaecks, Phys. Rev. Lett. **79**, 4982 (1997).
[21] U. Müller, T. Eckert, M. Braun, and H. Helm, Phys. Rev. Lett. **83**, 2718 (1999).
[22] I. Nevo *et al.*, Phys. Rev. A **76**, 022713 (2007).
[23] M. Schulz, R. Moshammer, D. Fischer, and J. Ullrich, J. Phys. B **37**, 4055 (2004).
[24] M. F. Ciappina, W. R. Cravero, M. Schulz, R. Moshammer, and J. Ullrich, Phys. Rev. A **74**, 042702 (2006).
[25] S. Otranto and R. E. Olson, J. Phys. B **39**, L175 (2006).
[26] M. Schulz, R. Moshammer, W. Schmitt, H. Kollmus, R. Mann, S. Hagmann, R. E. Olson, and J. Ullrich, Phys. Rev. A **61**, 022703 (2000).
[27] M. Schulz, T. Ferger, D. Fischer, R. Moshammer, and J. Ullrich, Phys. Rev. A **74**, 042705 (2006).
[28] M. Dürr, B. Najjari, M. Schulz, A. Dorn, R. Moshammer, A. B. Voitkiv, and J. Ullrich, Phys. Rev. A **75**, 062708 (2007).
[29] M. Schulz, M. Dürr, B. Najjari, R. Moshammer, and J. Ullrich, Phys. Rev. A **76**, 032712 (2007).
[30] S. Keller, B. Bapat, R. Moshammer, J. Ullrich, and R. M. Dreizler, J. Phys. B **33**, 1447 (2000).
[31] J. N. Silverman, O. Platas, and F. Matsen, J. Chem. Phys. **32**, 1402 (1960).
[32] L. G. Gerchikov and S. A. Sheinermann, J. Phys. B **34**, 647 (2001).
[33] C. DalCappello and H. LeRouzo, Phys. Rev. A **43**, 1395 (1991).
[34] B. Bapat *et al.*, J. Phys. B **32**, 1859 (1999).
[35] M. Brauner, J. S. Briggs, and H. Klar, J. Phys. B **22**, 2265

(1989).
[36] F. Maulbetsch and J. S. Briggs, J. Phys. B **26**, 1679 (1993).
[37] J. Berakdar and J. S. Briggs, Phys. Rev. Lett. **72**, 3799 (1994).
[38] J. Berakdar, Phys. Rev. A **53**, 2314 (1996).
[39] J. Berakdar, Phys. Rev. A **54**, 1480 (1996).
[40] S. Zhang, J. Phys. B **33**, 3545 (2000).
[41] J. R. Götz, M. Walter, and J. S. Briggs, J. Phys. B **38**, 1569 (2005).
[42] L. Gulyás, A. Igarashi, and T. Kirchner, Phys. Rev. A **74**, 032713 (2006).
[43] W. H. Press, S. A. Teukolsky, W. T. Vetterling, and B. P. Flannery, *Numerical Recipes in Fortran: The Art of Scientific Computing*, 2nd ed. (Cambridge, University Press, Cambridge, England, 1992).
[44] J. Ullrich, R. Moshammer, R. Dörner, O. Jagutzki, V. Mergel, H. Schmidt-Böcking, and L. Spielberger, J. Phys. B **30**, 2917 (1997).
[45] D. S. F. Crothers and R. McCarroll, J. Phys. B **20**, 2835 (1987).
[46] R. Shingal and C. D. Lin, J. Phys. B **24**, 251 (1991).